Letter

Multiphoton-dressed Rydberg excitations in a microwave cavity with ultracold Rb atoms

J. D. Massayuki Kondo [1,2] Seth T. Rittenhouse [3,4,5] Daniel Varela Magalhães [2] Vasil Rokaj [4,6]
S. I. Mistakidis [4,7] H. R. Sadeghpour [4] and Luis Gustavo Marcassa [2]

[1]*Departamento de Física, Universidade Federal de Santa Catarina, Florianópolis 88040-900, SC, Brasil*
[2]*Instituto de Física de São Carlos, Universidade de São Paulo, Caixa Postal 369, 13560-970 São Carlos, SP, Brasil*
[3]*Department of Physics, the United States Naval Academy, Annapolis, Maryland 21402, USA*
[4]*ITAMP, Center for Astrophysics|Harvard & Smithsonian, Cambridge, Massachusetts 02138, USA*
[5]*Institute of Theoretical Physics, Institute of Physics, University of Amsterdam, Science Park 904, 1098 XH Amsterdam, The Netherlands*
[6]*Department of Physics, Harvard University, Cambridge, Massachusetts 02138, USA*
[7]*Department of Physics, Missouri University of Science and Technology, Rolla, Missouri 65409, USA*

(Received 23 July 2024; revised 8 October 2024; accepted 12 November 2024; published 2 December 2024)

We investigate magneto-optical trap-loss spectroscopy of Rydberg excited ^{85}Rb ($66 \leqslant n \leqslant 68\, S_{1/2}$) atoms, placed inside a tailored microwave cavity. The cavity frequency at 13.053 GHz is in resonance with the $67S_{1/2} \rightarrow 66P_{3/2}$ transition, inducing a ladder multiphoton microwave Rydberg absorption and emission. The observed spectra are modeled with an extended Jaynes-Cummings formalism that accounts for nonlinear multiphoton absorption from and emission into the cavity, the loss from the trap due to Rydberg excitation, and cavity imperfection. We calculate the average photons in each spectral feature and find evidence for fractional photon emission into the cavity modes within the loss spectra. The microwave cavity Rydberg spectroscopy in this work provides key insights for advancing Rydberg-based sensors, quantum gates in hybrid systems, and the broader development of quantum technologies.

DOI: 10.1103/PhysRevA.110.L061301

Rydberg excitation in a cavity has a celebrated history in the emergence of cavity quantum electrodynamics (cQED). The Purcell effect [1] occurs when an increase in the local density of microwave (MW) photons leads to enhanced spontaneous emission. Initial observations were made on sodium atomic beams by enhancing [2–5] and suppressing [6,7] spontaneous emission. Additional experiments observed deviations in the Rydberg state lifetime in ultracold samples due to geometrical dependencies of the trapping vacuum chamber [8–10], showing a direct relation between black body radiation spectra and allowed cavity modes [8,11,12].

A well-tuned MW cavity can be used as a diagnostic tool to characterize cold plasma densities and temperatures [13]. More recently, cold Rydberg atoms interacting with MW cavity photons have been proposed to build a MW-to-optical converter via four-wave and six-wave mixing [14,15] and create quantum transducers from millimeter wave to optical field in a hybrid superconductor cryogenic resonator with ultracold Rb atoms [16,17]. MW resonators and cavities have also been applied in combination with electromagnetically induced transparency (EIT) to enhance MW electrometry in thermal samples [18–20].

Advances in Rydberg field sensors [21,22] and Rydberg-based logic gates [23,24] require a more thorough understanding of the intricacies of MW dressing of Rydberg states. Also, precision sensing of classical fields beyond the standard quantum limit [25] requires nonclassical states, such as squeezed and cat states [25–27].

We use an ultracold sample of ^{85}Rb held in a magneto-optical trap (MOT) placed inside a MW cavity to excite $nS_{1/2}$ Rydberg states ($66 \leqslant n \leqslant 68$). An extended Jaynes-Cummings model based on a multilevel multi-MW-photon formalism captures the details of the interaction of the MW cavity with the Rydberg atom excitation and identifies the multiphoton processes in the Rydberg fluorescence loss spectra. The model accounts for the loss of atoms from the cavity and faithfully reproduces, without any free parameters, the main features of the observed spectra. We calculate the average photon number for each spectral peak and find evidence for fractional photon emission into the cavity modes.

The ^{85}Rb MOT is loaded from an atomic vapor cell at room temperature and operates in a stainless steel chamber with a background pressure below 10^{-9} torr. Under normal conditions, it traps approximately 10^7 atoms at a density of about 10^{10} cm^{-3}. The trapping laser beam is red-tuned from the $5S_{1/2}, F = 3 \rightarrow 5P_{3/2}, F' = 4$ atomic transition, with an average Rabi frequency $\Omega_{\mathrm{MOT}}/2\pi$ of 13 MHz, detuned by $\delta \approx -2.1\Gamma$, where $\Gamma/2\pi = 5.9$ MHz. Figure 1(a) shows the ^{85}Rb energy states involved in trapping, cooling, and excitation of a nS Rydberg state. The repumping laser beam is resonant with the $5S_{1/2}, F = 2 \rightarrow 5P_{3/2}, F' = 3$ atomic transition. The trapping light is frequency-locked to a thermally stabilized optical cavity shown in Fig. 1(b) [28], and the repumping laser frequency is stabilized using a compact saturation spectroscopy system. Another laser, operating at a wavelength of 480 nm with a 300 μm waist and 4 W/cm^2 intensity, is used to couple the $5P_{3/2}, F' = 4$ state with the $nS_{1/2}$ Rydberg states in the range $66 \leqslant n \leqslant 68$.

The targeted Rydberg states are motivated because the cavity is resonant with the $67S_{1/2} \rightarrow 66P_{3/2}$ transition,

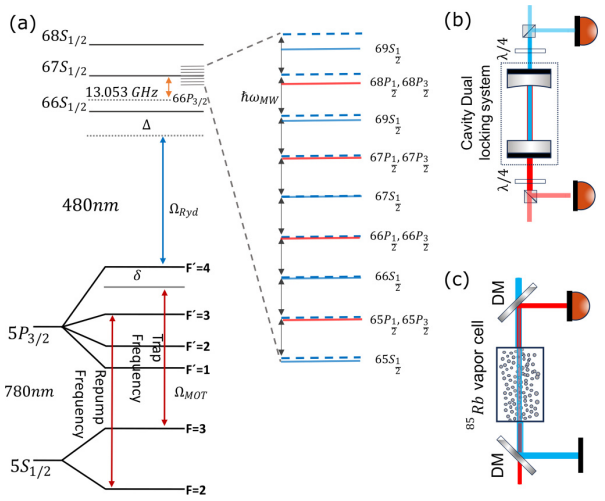

FIG. 1. (a) The ^{85}Rb energy diagram is shown along with a magnified version of the Rydberg spectrum near the $67S_{1/2}$ level. The total amount of excitations (matter plus MW photon) in the system is conserved. The dressed Rydberg basis set includes excitation from $|67S_{1/2}, n_0\rangle$ to $\ldots |66P_J, n_0+1\rangle, |67S_{1/2}, n_0\rangle, |67P_J, n_0-1\rangle, \ldots$ The number of cavity photons in the system is extracted by setting the Rabi frequency of the $67S_{1/2} \rightarrow 66P_{3/2}$ transition, equal to the splitting between the two most prominent features in the experimental spectrum. The number of states included is controlled by the number of photons emitted or absorbed by the atom. We find that the ac Stark energies for excitations near the $67S_{1/2}$ are converged by including all states with up to four photons emitted to or absorbed from the cavity. (b) Schematic representation of the EIT vapor reference cell, and (c) the thermally stabilized Fabry-Perot optical cavity (dual-locking system).

allowing the observation of multiphoton MW Rydberg transitions. This laser is frequency-locked to the same optical cavity after modulation by an electro-optical modulator, enabling precise scanning of the blue Rydberg laser in frequency steps as short as 100 kHz. The frequency of the Rydberg laser can be continuously monitored and calibrated using an EIT signal from a reference vapor cell held at ambient temperature [see Fig. 1(c)]. The 780 nm probe beam is provided by the trapping laser through the use of an acoustic-optical modulator (AOM), such that its detuning is set to zero ($\delta = 0$) with respect to the trapping transition. As the 480 nm laser scans over the EIT $nS_{1/2}$ resonances, its zero detuning ($\Delta = 0$) is set at the $5P_{3/2}, F = 4 \rightarrow nS_{1/2}$ transition.

As for a specific resonant blue laser detuning Δ, a number of Rydberg excitations can dynamically depopulate the atomic trap while background ground-state cold atoms are replenishing it in a constant rate. Toggling the blue laser during 50 ms proved to be sufficient for measuring the differences in MOT fluorescence signal and allows it to reach a steady-state population. The time sequence implemented is presented in Fig. 2. The fluorescence signal is acquired by a fast photodiode and fed to a boxcar rapid integrator, using two integration time windows of 15 μs each. Firstly, an N1 integration is performed just after turning the Rydberg laser on, and secondly, an N2 integration is carried just before turning it off, with the MOT

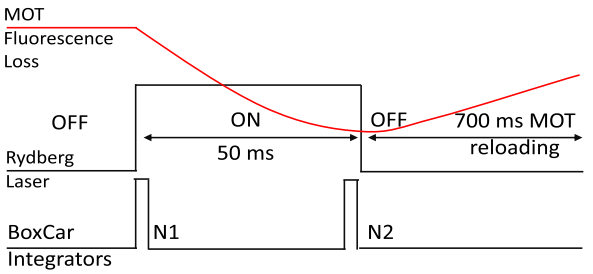

FIG. 2. Schematic of the experimental time sequence. The MOT fluorescence signal is acquired via boxcar integration electronics.

reloaded for 700 ms before the next iteration. The ratio N2/N1 was recorded for every Δ and accounted for the eventual MOT population fluctuations with an average of four measurements per experimental point.

The full level scheme of the system is illustrated in Fig. 1(a). The 13.053 GHz MW cavity mode is resonant with the $67S_{1/2} \leftrightarrow 66P_{3/2}$ Rydberg transition. The detailed experimental setup is described in the Supplemental Material [29]. Moreover, the $nS_{1/2}$ state is nearly halfway between the $(n-1)P_J$ and the nP_J states. This implies that the cavity is almost resonant with the $67S_{1/2} \leftrightarrow 67P_{3/2}$ transition, and thus can also drive the transition to the $67P_{3/2}$ state. The small spin-orbit splitting at high principal quantum number [30] necessitates the inclusion of the $nP_{1/2}$ states in our theoretical model (see below). Because the Rydberg states are not trapped by the MOT, they are observed as a loss signal from the cold atomic gas, which we shall model as a non-Hermitian loss. As a result, the corresponding Hamiltonian for the Rydberg atom excitation in the MW cavity is described by an extended (multilevel), non-Hermitian Jaynes-Cummings model,

$$\hat{H}_{\rm MW} = \hbar\omega_{\rm MW}\hat{a}^\dagger\hat{a} + \frac{\hbar}{2}(\hat{\Sigma}^+\hat{a} + \hat{\Sigma}^-\hat{a}^\dagger) + \hat{H}_{\rm Ryd}. \quad (1)$$

The operators $\hat{a}$ ($\hat{a}^\dagger$) annihilate (create) cavity photons, and $\hat{H}_{\rm Ryd}$ is the uncoupled Rydberg Hamiltonian:

$$\hat{H}_{\rm Ryd} = \sum_{nLJ}\left(-\frac{E_{\rm Ryd}}{(n-\mu_{LJ})^2} - i\hbar\frac{\gamma}{2}\right)|nLJ\rangle\langle nLJ|. \quad (2)$$

Here, μ_{LJ} denotes the Rydberg quantum defect [30] for orbital and total electron angular momenta (L and J), $E_{\rm Ryd}$ is the Rydberg constant, and γ represents the phenomenological loss rate of Rydberg atoms from the trap. In Eq. (1), $\hat{\Sigma}^+ = (\hat{\Sigma}^-)^\dagger$ is the operator representing the excitation of a Rydberg state through the absorption (emission) of a photon. Since the nD_J states are far detuned from the cavity, we only consider the nP_J and $nS_{1/2}$ states here. With this restriction the excitation operator reads

$$\hat{\Sigma}^+ = \sum_{n,J}\left(\Omega_J^{(n+1,n)}|(n+1)S_{1/2}\rangle\langle nP_J| + \Omega_J^{(n,n)}|nP_J\rangle\langle nS_{1/2}|\right), \quad (3)$$

where $\Omega_J^{(n',n)} = \sqrt{\frac{2\hbar\omega_{\rm MW}}{\varepsilon_0 V}}\langle n'S_{1/2}|\hat{d}|nP_J\rangle$ is the single-photon Rabi frequency, ε_0 is the vacuum permittivity, and V is the effective volume of the cavity mode. Because $\Omega_J^{(n+1,n)}$ varies

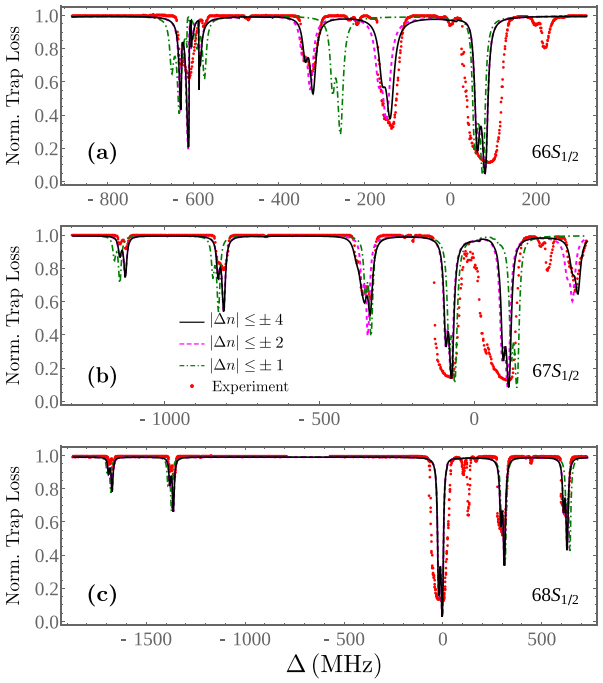

FIG. 3. Normalized trap-loss rate obtained from the extended Jaynes-Cummings model accounting for one, two, or four photons absorbed from or emitted to the cavity (i.e., $|\Delta n| \leqslant 1$, 2, or 4, respectively, as labeled in the legend) for varying Rydberg laser detuning Δ; for (a) $66S_{1/2}$, (b) $67S_{1/2}$, and (c) $68S_{1/2}$. Each resonance has a double peak structure with a separation of ∼13 MHz which originates from the Autler-Townes splitting of the MOT laser, coupling the $5S_{1/2}$ and $5P_{3/2}$ states [31]. In all cases, the respective experimental curves are provided showing good agreement with the theoretical predictions.

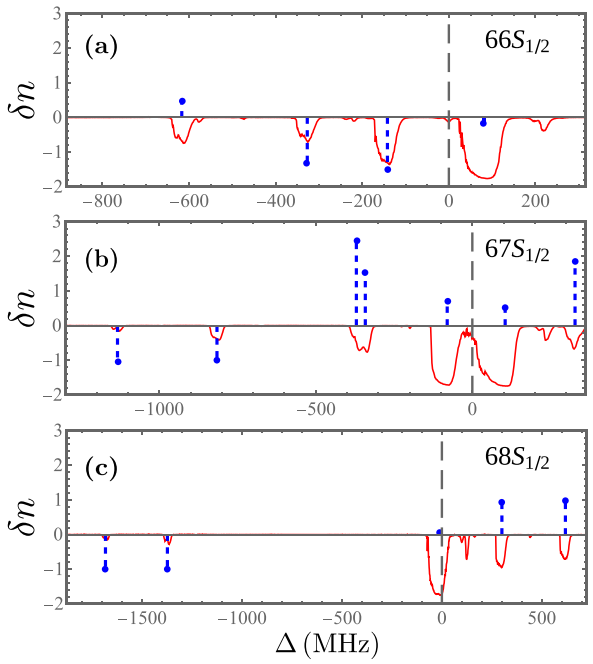

FIG. 4. Average number of photons emitted into ($\delta n > 0$) or absorbed from ($\delta n < 0$) the cavity for each state. The height of the vertical dashed lines indicate the average photon number for each observed spectral feature. Red lines represent the experimental spectrum corroborating the location of the resonances. The cases of the (a) $66S_{1/2}$, (b) $67S_{1/2}$, and (c) $68S_{1/2}$ states are shown with respect to the Rydberg laser detuning Δ. The MW cavity is driven at 32.8% of the maximum driving power, resulting in a MW electric field amplitude of 77.5 mV/cm.

by less than 10% over the range of principal quantum numbers considered here, we treat $\Omega_J^{(n',n)}$ to be independent of n, i.e., $\Omega_J^{(n+1,n)} \approx \Omega_J^{(n,n)} \approx \Omega_J^{(67,66)} = \Omega_J$. Incorporating the two-photon excitation from the $|5S_{1/2}\rangle$ to the $|nS_{1/2}\rangle$ Rydberg state, we predict the atom loss rate from the MOT [29].

The final fraction of atoms remaining in the trap after a long Rydberg pulse reads

$$\frac{N}{N_0} = \sqrt{1 + \left(\frac{\bar{\Gamma}_0/\gamma}{2\eta}\right)^2} - \frac{\bar{\Gamma}_0/\gamma}{2\eta},$$

where N_0 is the number of trapped atoms at the start of the pulse, $\bar{\Gamma}_0$ is the rate at which atoms are lost from the trap averaged over a Lorentzian cavity line profile, and $\eta = 0.0125$ is a fitting parameter which can be thought of as approximately the fraction of atoms that would remain if the full Rydberg loss rate, $\bar{\Gamma}_0 = \gamma$, were to be achieved.

Figure 3 illustrates a comparison of the experimentally observed trap-loss spectra for different initial Rydberg states, $66S_{1/2}$, $67S_{1/2}$, and $68S_{1/2}$, and the theory predictions for various cutoffs of the number of photons exchanged with the cavity ($|\Delta n| \leqslant 1$, 2, or 4), where $|\Delta n|$ is the number of exchanged photons. To examine the role of photon number in each spectral line, our theory accounts for processes involving one, two, and more photons, at a cavity field amplitude of 77.5 mV/cm. For each Rydberg state, there is a hyperfine state observed to the blue of the central Rydberg line that is not included in the theoretical description. It can be readily seen that many of the features for the $67S_{1/2}$ excitation spectrum depicted in Fig. 3(b) are approximately described by the inclusion of single-photon transitions (i.e., only accounting for the $66P_{1/2,3/2}$ and $67P_{1/2,3/2}$ states in the Rydberg basis beyond the $67S_{1/2}$ state). Importantly however, in the spectra presented in Fig. 3 we observe phenomena which require the participation of higher-photon processes. The resonance appearing at a detuning of +328 MHz is only present in the theoretical curves which include two or more photon processes. There is also a state at a detuning of −370 MHz (apparent as an additional shoulder to the red of the line at −350 MHz) in Fig. 3(b) which is only accounted for when three or more photon processes are included. Notice that the location of all states in the spectrum is numerically converged only when including higher multiphoton processes.

To examine the multiphoton nature of these states, we calculate the average deviation in the number of MW cavity photons from their background number, n_0, $\delta n = \langle \hat{a}^\dagger \hat{a} \rangle - n_0$ for each cavity state. Figure 4 presents the average number of photons emitted into ($\delta n > 0$) or absorbed from ($\delta n < 0$) the cavity for each Rydberg line in the $66S_{1/2}$, $67S_{1/2}$, and

$68S_{1/2}$ spectra at the cavity field amplitude of 77.5 mV/cm. Note that the experimental spectrum (red lines) has been included in Fig. 4 solely as a reference to ease the identification of various resonances. The two resonances occurring at −142 and −327 MHz in Fig. 4(a) refer to Autler-Townes (AT) splitting and are shifted from the main AT lines in Fig. 4(b), by absorption of an additional photon from the cavity in the multiphoton process $66S_{1/2} \rightarrow 66P_{3/2} \rightarrow 67S_{1/2}$. The line at −631 MHz is a single-photon absorption to the $65P_{3/2}$ state, and the main Rydberg line is ac Stark blue-shifted. In Fig. 4(b), the resonances at +328 MHz and the one at −370 MHz are two- and three-photon processes associated with the $|67S_{1/2}, n_0\rangle \rightarrow |66P_{3/2}, n_0 + 1\rangle \rightarrow |66S_{1/2}, n_0 + 2\rangle$ and additional $|66S_{1/2}, n_0 + 2\rangle \rightarrow |65P_{3/2}, n_0 + 3\rangle$ transitions, respectively. The resonance appearing at -342 MHz is largely a single-photon transition, $|67S_{1/2}, n_0\rangle \rightarrow |66P_{1/2}, n_0 + 1\rangle$, with some additional coupling to the $|66S_{1/2}, n_0 + 2\rangle$ state. The resonances in the detuning range from −1100 to −800 MHz are single-photon emission lines describing the transitions $|67S_{1/2}, n_0\rangle \rightarrow |67P_{3/2}, n_0 + 1\rangle$ and $|67S_{1/2}, n_0\rangle \rightarrow |67P_{1/2}, n_0 + 1\rangle$, respectively. Because the cavity is far detuned from any nP states near the $68S_{1/2}$ state, see Fig. 1(a), only single-photon emission into and absorption from the MW cavity are visible in Fig. 4(c).

An interesting feature in Fig. 4(b) is that there exist peaks which share one photon. This holds for the doublets in Fig. 4(b) around zero detuning and around −370 MHz. This phenomenon indicates the existence of nontrivial photon correlations between the states that share the photon excitation. The fractional photon occupation feature could potentially be utilized for sensitive electrometry, as the red and blue AT doublet in Fig. 4(b) will have different Stark shifts [32]. Additionally, the multiphoton nature of some resonances indicates that their transition amplitudes and positions will respond nonlinearly to external fields. This nonlinearity renders them exceptionally sensitive to environmental fields, making them promising candidates for high-precision field sensors.

To inspect the type of photon correlations, we employ the standard two-level Jaynes-Cummings model. The dressed Jaynes-Cummings states for zero detuning are $|\pm, n_0\rangle = \frac{1}{\sqrt{2}}(|g, n_0 + 1\rangle \pm |e, n_0\rangle)$, where $|g\rangle$ and $|e\rangle$ are the energetically lowest and highest states, respectively, in the two-level system [33], with n_0 photons. The dressed states have noninteger photon numbers $\langle \hat{a}^\dagger \hat{a} \rangle_{\pm n_0} = n_0 + \frac{1}{2}$ and they share a photon.

A measure of photon correlation is the Mandel Q parameter [33],

$$Q = \frac{\langle (\Delta \hat{n})^2 \rangle - \langle \hat{n} \rangle}{\langle \hat{n} \rangle}, \tag{4}$$

where $\hat{n} = \hat{a}^\dagger \hat{a}$ is the photon number operator and $\langle (\Delta \hat{n})^2 \rangle \equiv \langle \hat{n}^2 \rangle - \langle \hat{n} \rangle^2$ represents its variance. If $-1 \leqslant Q < 0$, the photons follow sub-Poissonian statistics, a signature of quantum light without a classical analog [33–35]. For the Jaynes-Cummings Hamiltonian, $Q_{\pm n_0} = -\frac{n_0 + \frac{1}{2}}{n_0 + \frac{1}{2}}$, with $Q_{\pm n_0} \underset{n_0 \gg 1}{\rightarrow} -1$. It is then plausible that the spectral peaks in Fig. 4(b) featuring noninteger photon numbers exhibit nonclassical photon correlations.

We explored the direct excitation of dressed Rydberg states in an ultracold ^{85}Rb sample held inside a three-dimensional MW cavity and observed multiphotonic MW cavity exchange. For this we investigate the excitation spectra around three specific Rydberg states, $66S_{1/2}$, $67S_{1/2}$, and $68S_{1/2}$, by performing fluorescence trap-loss spectroscopy. The cavity was engineered to match the energy difference for the transition $67S_{1/2} \rightarrow 66P_{3/2}$ and MW field was supplied to the chamber by an intracavity antenna. We were able to describe the Rydberg excitation spectra by using a multilevel Jaynes-Cummings model. By taking into account multiphoton processes of emission and absorption within the MW resonant cavity, and including a precise trap-loss description, the model greatly reproduces the observed spectra.

We calculated the average number of MW photons emitted to or absorbed from the cavity for each spectral resonance. Because the transition oscillator strengths to the dressed states are necessarily nonlinear in response to environmental changes, these states could be potential candidates for quantum sensing. It would be interesting to probe quantum effects due to the cavity for the generation of specific dressed states, as superposition of photon excitations. The fractional MW photon numbers in the Rydberg AT lines in Fig. 4(b) may herald the creation of nonclassical photon states or antibunching. Further investigations of the MW photon statistics by cooling the cavity are warranted.

This work is supported by Grants No. 2019/10971-0 and No. 2021/06371-7, São Paulo Research Foundation (FAPESP), and CNPq (305257/2022-6). It was also supported by the Army Research Office Grant No. W911NF-21-1-0211. V.R., S.I.M., H.R.S., and S.T.R. acknowledge support from the NSF through a grant for ITAMP at Harvard University.

[1] E. M. Purcell, H. C. Torrey, and R. V. Pound, Phys. Rev. **69**, 37 (1946).
[2] P. Goy, J. M. Raimond, M. Gross, and S. Haroche, Phys. Rev. Lett. **50**, 1903 (1983).
[3] S. Haroche and J. Raimond, *Radiative Properties of Rydberg States in Resonant Cavities* (Academic Press, New York, 1985), pp. 347–411.
[4] S. Haroche and D. Kleppner, Phys. Today **42**(1), 24 (1989).
[5] S. Haroche, AIP Conf. Proc. **464**, 45 (1999).
[6] D. Kleppner, Phys. Rev. Lett. **47**, 233 (1981).
[7] R. G. Hulet, E. S. Hilfer, and D. Kleppner, Phys. Rev. Lett. **55**, 2137 (1985).
[8] M. Archimi, C. Simonelli, L. Di Virgilio, A. Greco, M. Ceccanti, E. Arimondo, D. Ciampini, I. I. Ryabtsev, I. I. Beterov, and O. Morsch, Phys. Rev. A **100**, 030501(R) (2019).
[9] J. Tallant, D. Booth, and J. P. Shaffer, Phys. Rev. A **82**, 063406 (2010).

[10] B. Magnani, C. Mojica-Casique, and L. G. Marcassa, J. Phys. B: At., Mol. Opt. Phys. **53**, 064004 (2020).
[11] A. Reiser and L. Schächter, Phys. Rev. A **87**, 033801 (2013).
[12] M. Mack, J. Grimmel, F. Karlewski, L. Sárkány, H. Hattermann, and J. Fortágh, Phys. Rev. A **92**, 012517 (2015).
[13] M. A. W. van Ninhuijs, K. A. Daamen, J. Beckers, and O. J. Luiten, Rev. Sci. Instrum. **92**, 013506 (2021).
[14] J. P. Covey, A. Sipahigil, and M. Saffman, Phys. Rev. A **100**, 012307 (2019).
[15] J. Han, T. Vogt, C. Gross, D. Jaksch, M. Kiffner, and W. Li, Phys. Rev. Lett. **120**, 093201 (2018).
[16] A. Kumar, A. Suleymanzade, M. Stone, L. Taneja, A. Anferov, D. I. Schuster, and J. Simon, Nature (London) **615**, 614 (2023).
[17] J. C. Bohorquez, R. Chinnarasu, J. Isaacs, D. Booth, M. Beck, R. McDermott, and M. Saffman, Phys. Rev. A **108**, 022805 (2023).
[18] C. L. Holloway, N. Prajapati, A. B. Artusio-Glimpse, S. Berweger, M. T. Simons, Y. Kasahara, A. Alù, and R. W. Ziolkowski, Appl. Phys. Lett. **120**, 204001 (2022).
[19] B. Liu, L.-H. Zhang, Z.-K. Liu, Q.-F. Wang, Y. Ma, T.-Y. Han, Z.-Y. Zhang, S.-Y. Shao, J. Zhang, Q. Li, H.-C. Chen, D.-S. Ding, and B.-S. Shi, arXiv:2404.06915.
[20] M. T. Simons, A. H. Haddab, J. A. Gordon, D. Novotny, and C. L. Holloway, IEEE Access **7**, 149936 (2019).
[21] C. G. Wade, N. Šibalić, N. R. de Melo, J. M. Kondo, C. S. Adams, and K. J. Weatherill, Nat. Photon. **11**, 40 (2017).
[22] C. G. Wade, M. Marcuzzi, E. Levi, J. M. Kondo, I. Lesanovsky, C. S. Adams, and K. J. Weatherill, Nat. Commun. **9**, 3567 (2018).
[23] S. Ebadi *et al.*, Science **376**, 1209 (2022).
[24] Y.-Y. Jau, A. M. Hankin, T. Keating, I. H. Deutsch, and G. W. Biedermann, Nat. Phys. **12**, 71 (2016).
[25] A. Facon, E.-K. Dietsche, D. Grosso, S. Haroche, J.-M. Raimond, M. Brune, and S. Gleyzes, Nature (London) **535**, 262 (2016).
[26] C. L. Degen, F. Reinhard, and P. Cappellaro, Rev. Mod. Phys. **89**, 035002 (2017).
[27] S. Gleyzes, S. Kuhr, C. Guerlin, J. Bernu, S. Deléglise, U. Busk Hoff, M. Brune, J.-M. Raimond, and S. Haroche, Nature (London) **446**, 297 (2007).
[28] D. Rodriguez Fernandez, M. A. Lefran Torres, M. R. Cardoso, J. D. M. Kondo, M. Saffman, and L. G. Marcassa, Appl. Phys. B **130**, 60 (2024).
[29] See Supplemental Material at http://link.aps.org/supplemental/10.1103/PhysRevA.110.L061301 for details of the experimental setup, fluorescence measurement, and electrometry calibration.
[30] W. Li, I. Mourachko, M. W. Noel, and T. F. Gallagher, Phys. Rev. A **67**, 052502 (2003).
[31] X. Wang, X. Hou, F. Lu, R. Chang, L. Hao, W. Su, J. Bai, J. He, and J. Wang, AIP Adv. **13**, 035126 (2023).
[32] J. A. Gordon, C. L. Holloway, A. Schwarzkopf, D. A. Anderson, S. Miller, N. Thaicharoen, and G. Raithel, Appl. Phys. Lett. **105**, 024104 (2014).
[33] C. Gerry and P. Knight, *Introductory Quantum Optics* (Cambridge University Press, Cambridge, 2004).
[34] L. Mandel, Opt. Lett. **4**, 205 (1979).
[35] D. M. Welakuh, M. Ruggenthaler, M.-L. M. Tchenkoue, H. Appel, and A. Rubio, Phys. Rev. Res. **3**, 033067 (2021).